Additional α-glucosidase inhibitors from Malbranchea flavorosea (Leotiomycetes, Ascomycota)

By: Daniela Rebollar-Ramos, Martha L. Macías-Ruvalcaba, Mario Figueroa, Huzefa A. Raja, Martín González-Andrade, and Rachel Mata

Made available courtesy of Springer Nature: http://dx.doi.org/10.1038/s41429-018-0075-6

Abstract:

From the rice-based culture of *Malbranchea flavorosea*, three new compounds namely flavoroseoside B (5-desoxy-5-chloro-flavoroseoside) (**2**), 4-hydroxy-2-*O*-α-ribofuranosyl-5-methylacetophenone (**3**), and (*S*)-3,4-dihydro-3-(1*H*-indol-3-ylmethyl)-4-methyl-1*H*-1,4-benzodiazepine-2,5-dione (**4**), along with three known compounds, rosigenin (**5**), massarilactone B (**6**), and riboxylarinol B (**7**) were obtained. The structures were determined by spectroscopic methods. Compound **4** and its synthetic analog 3,4-dihydro-3-(1*H*-indol-3-ylmethyl)-1-methyl-1*H*-1,4-benzodiazepine-2,5-dione (**9**) inhibited the activity of *Ruminococus obeum* α-glucosidase enzyme. Molecular docking and dynamic studies revealed that compounds **4** and **9** might bind to this α-glucosidase at the catalytic center. Phylogenetic analysis using internal transcribed spacer region revealed that *Malbranchea flavorosea* ATCC 34529 is related to *Myxotrichum* spp.

Keywords: natural products | small molecules | *Malbranchea flavorosea* | enzymatic assay | fungi

Article:

Introduction

The global prevalence of type II diabetes has risen considerably in the last 5 years; the International Diabetes Federation estimates that there are 425 million people with this disease, which is among the top 10 causes of death worldwide. Also, there is a significant economic impact due to the high cost of its treatment [1]. Hence, new therapies for diabetes are very relevant nowadays. Metformin is the first-line medication for the treatment of type II diabetes mellitus, while the use of other well-established agents varies in different regions. In areas with large consumption of complex carbohydrates, α-glucosidase inhibitors are widely used. These agents competitively and reversibly inhibit α-glucosidase enzymes located in the brush border of

the small intestine, delaying the digestion of starch and sucrose and the consequent postprandial blood glucose excursions [2].
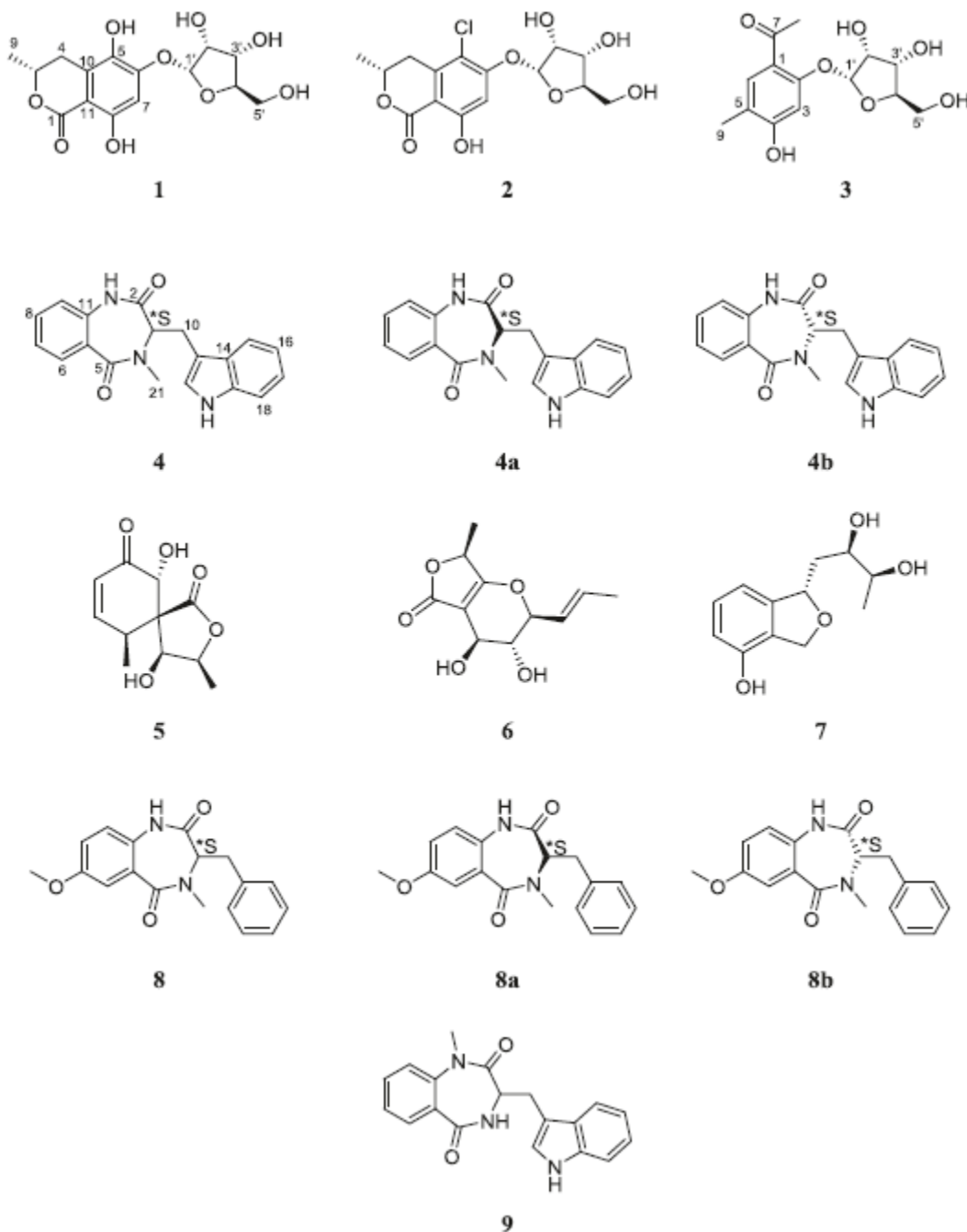
Figure 1. Structures of compounds 1–7 isolated from the fungus M. flavorosea, and related compounds 8 and 9

As part of an effort to discover α-glucosidase inhibitor lead compounds from fungi and plants [3, 4], we investigated Malbranchea flavorosea Sigler and Carmichael (Myxotrichaceae) in a previous work and identified flavoroseoside (1) (Fig. 1), 8-chloroxylarinol A, xylarinols A and B, massarigenins B and C, and clavatol [5]. Massarigenin C showed a good α-glucosidase

inhibitory activity both in vivo and in vitro. Therein, we report the further chemical investigation of a rice-based culture of the fungus M. flavorosea, the α-glucosidase inhibitory activity of the isolates and taxonomic features of the fungus.

Results and discussion

Fungal strain and identification

The fungal strain Malbranchea flavorosea Sigler & Carmichael (type strain: ATCC 34529) [6] was obtained from the American Type Culture Collection. Species in the genus Malbranchea are commonly isolated from soil, but also dung and cellulose; there are ~22 species reported in the literature [7]. Members of Malbranchea are phylogenetically affiliated to the Onygenaceae, Onygenales, Eurotiomycetes Ascomycota [8, 9], however, not all Malbranchea spp. have been identified based on molecular data and, for a number of species, the ITS barcodes are lacking. For M. flavorosea, one partial nuclear large subunit gene sequence is deposited in NCBI GenBank (AB359419), but since no published reference is associated with this accession number, the authenticity of the sequence cannot be verified. Therefore, we sequenced the type isolate of M. flavorosea (ATCC 34529) for the internal transcribed spacer region (ITS1-5.8S-ITS2), which is designated as the barcoding marker for fungi [10] to predict its phylogenetic relationship with closest members in NCBI GenBank. DNA extraction, PCR, Sanger sequencing, and molecular phylogenetic analysis using maximum likelihood were performed following protocols that have been recently described [11]. The ITS sequences obtained (n = 4) were BLAST searched in GenBank to verify the identity and sequence homology with other similar ITS sequences in the public database. Based on a BLAST search of the NCBIs GenBank nucleotide database, the closest hit using the ITS sequence was Myxotrichum stipitatum [GenBank AF062816; Identities 479/493 (97%); Gaps 3/493 (0%)] [12], followed by Myxotrichum stipitatum strain SFCF20120912-11 [Gen-Bank KF313096; Identities 493/514 (96%); Gaps 3/514 (0%)] [13], then by Myxotrichum carminoparum UAMH 159 [GenBank AF062812; Identities 459/494 (93%); Gaps 3/494 (0%] [12], and then followed by Myxotricheaceae [GenBank KC007174; Identities 779/895 (87%); Gaps (32/895) (3%)] [14]. To elucidate the phylogenetic placement of strain ATCC 34529, we downloaded the top matches of the ITS sequences from GenBank and carried out a phylogenetic analysis. Maximum Likelihood phylogeny indicated that strain ATCC 34529 showed phylogenetic affiliations to Myxotrichum spp. (Fig. 2). Members of Myxotrichum (Myxotrichaceae Locq. & Currah) were previously placed and considered related to the Onygenales, Eurotiomycetes; however, molecular phylogenetic studies place them in an uncertain, isolated position within the Leotiomycetes [12, 15]. Thus, our data suggest that M. flavorosea shows phylogenetic relatedness to Myxotrichum spp. (incertae sedis Leotiomycetes, Ascomycota), which was reported by Sigler and Carmichael (1976) in their monograph on Malbranchea spp [6]. An older study on Malbranchea also indicated that M. flavorosea may have a Myxotrichum sexual state [16]. This analysis is preliminary and further sequencing of both ribosomal and protein-coding loci, along with additional phylogenetic analysis of Malbranchea, is necessary to better understand the phylogenetic disposition of this fungus. The sequence data are deposited in GenBank with accession numbers: MH037295, MH037296, MH037297, and MH037298.
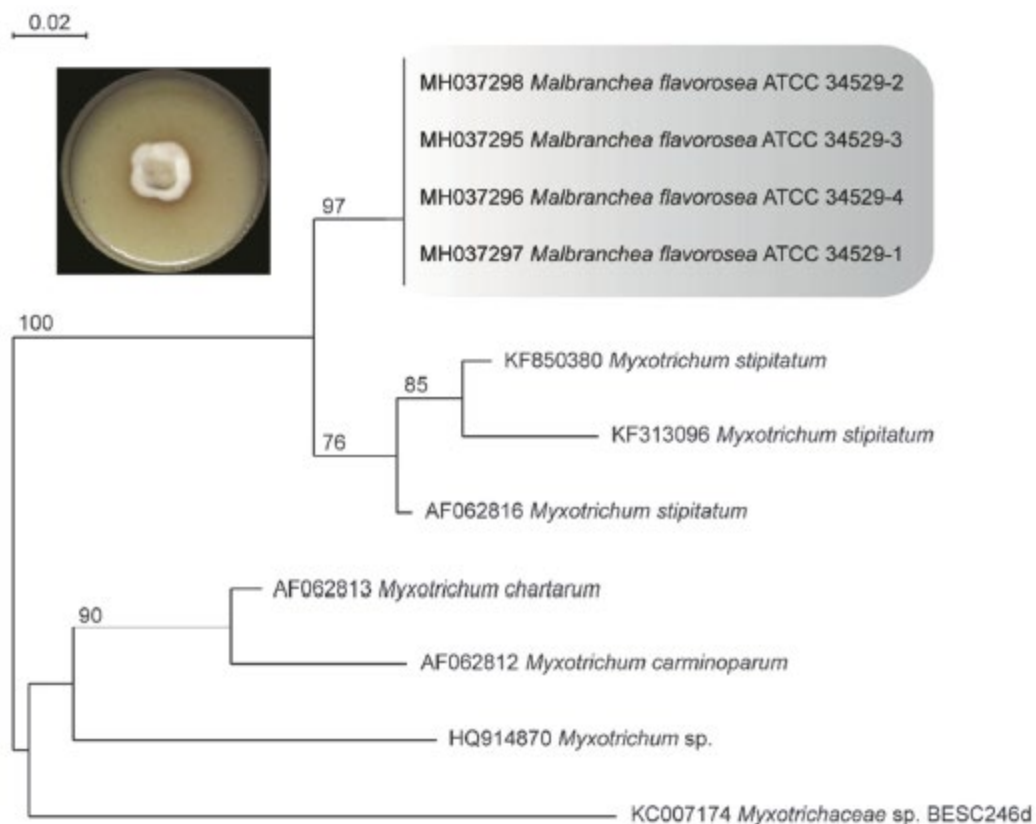
Figure 2. Phylogram of the most likely tree (−lnL = 1415.05) from a PHYML analysis of 11 taxa based on the ITS region (533 bp). Numbers refer to PHYML bootstrap support values ≥ 70% based on 1000 replicates. Malbranchea flavorosea (ATCC 34529) is phylogenetically related to Myxotrichum stipitatum (incertae sedis Leotiomycetes, Ascomycota). A 14-d-old culture on oatmeal media is shown. Bar indicates nucleotide substitutions per site

Isolation of compounds

Conventional fractioning of an active organic extract from the rice-based culture of M. flavorosea led to the isolation of three new compounds, flavoroseoside B (5-desoxy-5-chloro-flavoroseoside) (2), 4-hydroxy-2-O-α-D-ribofuranosyl-5-methylacetophenone (3), and (3 S)-3,4-dihydro-3-(1H-indol-3-ylmethyl)-4-methyl-1H-1,4-benzodiazepine-2,5-dione (4), along with rosigenin (5) [17], massarilactone B (6) [18], and riboxylarinol B (7) [19] (Fig. 1).

Compound 2 was isolated as an optically active colorless glassy solid. Its molecular formula was established by HRESIMS as $C_{15}H_{17}O_8Cl$, requiring 7 degrees of unsaturation. The presence of a chlorine atom in the molecule was consistent with the relative abundance of the $[M^+2]^+$ peak with respect to the molecular ion $[M^+]$. The IR spectrum showed a signal characteristic of chelated carbonyl (1664 cm^{-1}) and phenol (1241 cm^{-1}) groups. The NMR spectra (Table 1) showed strong similarities with those of flavoroseoside (1) [5]; comparative analyses revealed that the only difference was the chemical shift value of the signal attributed to C-5, which was diamagnetically shifted from δ_C 149.1 in 1 to δ_C 113.3 in 2, suggesting that the hydroxyl group in 1 was replaced by a chlorine atom in 2. Since the CD spectra of 1 and 2 were identical, the absolute configuration of the methyl group at C-3 was determined to be R. In addition, the

optical rotation sign was identical and the value was very similar of 2, suggesting that the ribofuranosyl unit also belongs to the D series.

Table 1. ^1H (700 MHz) and ^{13}C (175 MHz) NMR data for compound 2 in CD$_3$OD

Position	2	
	δ_C type	δ_H mult (J in Hz)
1	170.5, C	
3	76.1, CH	4.69 ddd (3.3, 6.3, 11.4)
4	32.7, CH$_2$	α, 3.29 dd (3.3, 16.9)
		β, 2.79 dd (11.4, 16.9)
5	113.3, C	
6	159.7. C	
7	103.4, CH	6.82 s
8	163.2, C	
9	20.4, CH$_3$	1.51 d (6.3)
10	139.4, C	
11	103.6, C	
1′	102.2, CH	5.75 d (4.4)
2′	72.9, CH	4.26 dd (4.4, 6.4)
3′	70.3, CH	4.12 dd (3.4, 6.4)
4′	88.2, CH	4.17 dd (3.4, 6.4)
5′	62.5, CH$_2$	α, 3.68 dd (3.7, 12.2)
		β, 3.64 dd (3.7, 12.2)

Table 2. ^1H (700 MHz) and ^{13}C (175 MHz) NMR data for compound 3 in CD$_3$OD

Position	3	
	δ_C type	δ_H mult (J in Hz)
1	115.2, C	
2	163.3, C	
3	103.5, CH	6.69 s
4	164.1, C	
5	120.5, C	
6	133.5, CH	7.64 d (1.1)
7	204.7, C	
8	26.5, CH$_3$	2.57 s
9	15.8, CH$_3$	2.22 d (1.1)
1′	101.7, CH	5.72 d (4.4)
2′	73.4, CH	4.25 ddd (2.2, 4.4, 6.2)
3′	70.9, CH	4.13 m
4′	88.1, CH	4.13 m
5′	63.1, CH$_2$	α, 3.72 dd (3.5, 12.2)
		β, 3.67 dd (3.5, 12.2)

Compound 3 was isolated as a brown oil. HRESIMS yielded the molecular formula $C_{14}H_{18}O_7$ with 6 degrees of unsaturation. Based on NMR data (Table 2), 3 was determined to be a glycoside closely related to clavatol, which was previously isolated from this fungus [5]. The main difference between the NMR spectra of clavatol and 3 were the presence of signals for an α-ribofuranosyl moiety and the replacement of the 3-methyl group signal at δ_H/δ_C 2.11/7.43 by that of an aromatic methine proton (δ_H/δ_C 6.69/103.5). All carbon signals were assigned according to the HSQC and HMBC correlations. The HMBC cross peaks of H-6 (δ_H 7.64) with C-2 (δ_C 163.3), C-4, (δ_C 164.1), C-7 (δ_C 204.7), and C-9 (δ_C 15.8), as well as those of H-3 (δ_H 6.69) with C-1 (δ_C 115.2) and C-5 (δ_C 120.5), corroborated the positions of the substituents along the aromatic core. The placement of the ribofuranosyloxy moiety at C-2 was confirmed by the HMBC correlation between H-1′ (δ_H 5.72) and C-2. Thus, compound 3 was characterized as 4-hydroxy-2-O-α-ribofuranosyl-5-methylacetophenone.

Table 3. ^{1}H (700 MHz) and ^{13}C (175 MHz) NMR data for compounds 4 (4a/4b) and 9 in CD$_3$OD

Position	4a		4b		9	
	δ_C type	δ_H mult (J in Hz)	δ_C type	δ_H mult (J in Hz)	δ_C type	δ_H mult (J in Hz)
2	171.7, C		173.1, C		171.2, C	
3	57.1, CH	4.52 dd (7.6, 7.6)	69.1, CH	4.46 dd (6.8, 10.4)	52.8, CH	4.09 dd (6.2, 8.2)
5	170.8, C		168.3, C		169.5, C	
6	131.7, CH	7.84 d (7.7)	132.4, CH	8.00 d (7.7)	129.3, CH	7.73 dd (1.4, 7.8)
7	133.7, CH	7.53 dd (7.5, 7.7)	134.1, CH	7.63 dd (7.4, 7.7)	132.5, CH	7.60 dd (7.8, 7.8)
8	125.9, CH	7.29 dd (7.5, 7.8)	125.8, CH	7.38 dd (7.4, 7.6)	125.5, CH	7.32m
9	122.1, CH	7.10m	121.6, CH	7.20m	122.0, CH	7.41 d (7.8)
10	23.1, CH$_2$	3.47m	25.5, CH$_2$	2.88 dd (10.4, 14.7)	23.8, CH$_2$	3.19 dd (8.2, 15.0)
				3.02 dd (6.8, 14.7)		3.46 dd (6.2, 15.0)
11	128.2, C		127.7, C		141.2, C	
12	137.1. C		137.9, C		128.1, C	
13	110.6, C		109.7, C		109.3, C	
14	128.4, C		128.1, C		127.0, C	
15	118.8, CH	7.44 d (8.0)	118.8, CH	7.44 d (7.9)	117.4, CH	7.42 d (7.8)
16	119.9, CH	6.96 dd (7.5, 8.0)	120.1, CH	7.03m	118.4, CH	6.93 dd (7.4, 7.8)
17	122.7, CH	7.07 dd (7.5, 7.9)	122.6, CH	7.10m	121.0, CH	7.05 dd (7.4, 7.5)
18	112.4, CH	7.33 d (7.9)	112.5, CH	7.33 d (8.1)	110.9, CH	7.32 d (7.5)
19	138.1, C		138.1, C		136.6, C	
20	124.1, CH	7.05 s	124.6, CH	6.90 s	123.5, CH	7.15 s
21	29.2, CH$_3$	3.15 s	39.8, CH$_3$	2.91 s	34.6, CH$_3$	3.43 s

Compound 4 was isolated as a white amorphous solid. The molecular formula was determined as $C_{19}H_{17}O_2N_3$ by HRESIMS, which accounted for 12 unsaturation degrees. The IR spectrum showed bands due to amide and phenyl groups (1683 and 1619 cm^{-1}). When the ^{13}C NMR spectrum was recorded in CD3OD at room temperature, 38 signals were observed rather than 19 as suggested by the molecular formula (Table 3). In the ^{1}H NMR spectrum, all signals were observed also in pairs in a 1:1 ratio. However, when the ^{1}H NMR was recorded in DMSO-d_6 at

50 °C, the two sets of signals merged into single resonances (Supplementary Information). Altogether, this information indicated that 4 existed as a mixture of two different stable conformers (4a/4b) at room temperature, and that the energy barrier for interconversion was significantly higher compared with the NMR time-scale. Comparative analysis of the NMR spectra of 4a/4b (Table 3) with those of 7-methoxycyclopeptin (8) [20] and related compounds [21] revealed strong similarities, albeit partial. Compound 8 is also a dipeptide of the benzodiazepinedione family, which at room temperature exists as a mixture of two conformers in a 5:4 ratio (8a/8b) [20]. The main differences observed in the NMR spectra of both compounds were the signals for the second amino acid and the presence of a methoxy group at the anthranilic derived residue. Thus, the signals for the phenylalanine residue in 8a/8b were replaced for those of a tryptophan residue in 4a/4b. On the other hand, the ABX system for the 3-methoxyanthranilic residue of 8a/8b was replaced by an AA′BB′ system of an unsubstituted anthranilic acid moiety in 4a/4b. The negative value of the optical rotation ($[\alpha]_D^{20} = -57.7°$) indicated that the absolute configuration of the only chiral center was S, suggesting that L-tryptophan was the precursor of 4a/4b. During the characterization process, the 1-methylated analog 9 was synthesized as described in the experimental section, and its NMR data (Table 3) was similar to that of the conformer mixture 4a/4b; however, the signals were not paired, suggesting that the energy barrier for interconversion of 9 was lower compared with the NMR time-scale.

Biological activity

Compounds 2–6 and 9 were tested against recombinant α- glucosidase with maltase-glucoamylase activity obtained from Ruminococcus obeum (Table 4; compounds 1 and 7 were not tested due to the paucity of sample) [22]. The benzodiazepinediones 4 and 9 displayed the best inhibitory activity against the enzyme ($IC_{50} = 1.33 \pm 0.05$ and 1.68 ± 0.07 mM, respectively), while the activity of 2, 3, and 5 was weak ($IC_{50} > 3$ mM). Recombinant R. obeum α-glucosidase is a structural homologue of human N-maltase-glucoamylase; and possesses a highly conserved catalytic domain [22]. So, it is possible to make better inferences regarding the potential in vivo effects in humans of any compound assayed with this enzyme. Compounds 4 and 9 were also tested against Saccharomyces cerevisiae α-glucosidase, showing a higher affinity for this enzyme ($IC_{50} = 0.19 \pm 0.02$ and 0.54 ± 0.05 mM, respectively). Thus, 4 and 9 possess a better sucrase inhibitory activity. Although this is the first report of benzodiazepinediones as α-glucosidase inhibitors, some dipeptides of the diketopiperazine family and a quinazolino-benzodiazepine metabolite were reported as α-glucosidase inhibitors [23, 24].

Docking and molecular dynamics

Molecular modeling studies indicate that the compounds with the highest affinity to the enzyme are 9, 2, and 4. Theoretical K_i values obtained from docking are shown in Table 4. According to the results of the docking analysis (Fig. 3), these compounds bind in the same site than acarbose (positive control); the amino acids involved in the interactions are: Asp197, Ile234, Tyr169, Trp271, Trp305, Asp307, Arg404, Trp417, Asp420, Phe453, and His478. Moreover, the energetic data (ΔG) obtained from the molecular dynamics (MD) trajectory analysis show that acarbose, 4 and 9 are the compounds that present the best binding (Table 4). These results agree with the experimental data obtained for this series of compounds. The root mean square

deviation (RMSD) obtained from the analysis of MD trajectories indicate the degree of conformational flexibility of the system (α-glucosidase-ligand complexes). Figure 4 shows the comparison of the RMSDs of the complexes α-glucosidase-acarbose, α-glucosidase-4 and α-glucosidase-9, which showed similar fluctuation. Figure 5 is a graphical representation of the trajectory of MD of the glucosidase-4 complex during 20 ns. This representation indicates how the compounds fluctuate in the catalytic site and are reoriented, just as the enzyme itself shows adjacent conformational changes. All the MD trajectories of the complexes are shown in movies in the Supplementary Information.

Table 4. Inhibition parameters (in vitro and in silico) of compounds 1–9 against α-glucosidases

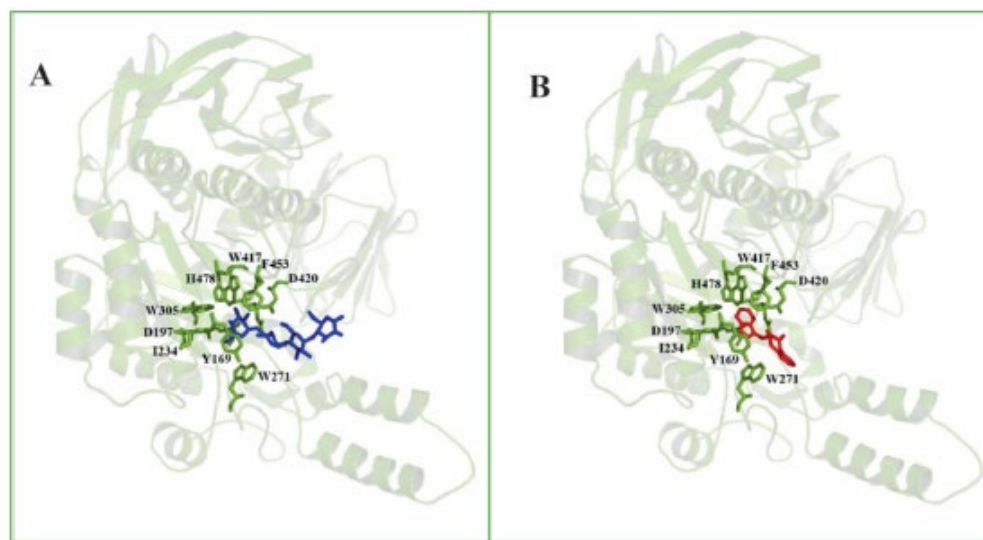| Compound	α-Ro				α-GHY
	IC_{50} (mM)	K_i (μM)	EFEB (kcal/mol)	ΔG (kcal/mol)	IC_{50} (mM)
1	NT	10.69	−6.78	−24.30	NT
2	>3	3.02	−7.53	−15.04	NT
3	>3	39.33	−6.01	−15.46	NT
4	1.33 ± 0.05	3.88	−7.38	−22.94	0.19 ± 0.02
5	>3	11.96	−6.72	−9.24	NT
6	»3	44.39	−5.99	−4.37	NT
7	NT	23.19	−6.32	−8.41	NT
8	NT	5.42	−7.18	−14.25	NT
9	1.68 ± 0.07	1.98	−7.78	−23.56	0.54 ± 0.05
Acarbose[a]	1.05 ± 0.02	0.29	−8.92	−31.00	1.22 ± 0.03

NT not tested; [a] Positive control

Figure 3. Structural model of complexes of α-glucosidase with acarbose (a) and 4 (b) from to docking study. α-Glucosidase represented in green cartoon and the amino acids involved in the catalytic site in green sticks. This figure was prepared using PyMOL
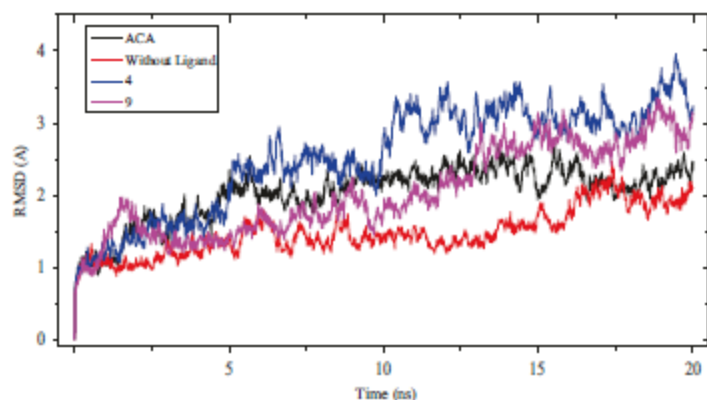
Figure 4. The RMSD and time plot for a 20 ns MD simulation. α-glucosidase with acarbose (ACA) (—, black line), α-glucosidase without ligand (—, red line), α-glucosidase-4 complex (—, blue line), and α-glucosidase-9 complex (—, pink line)
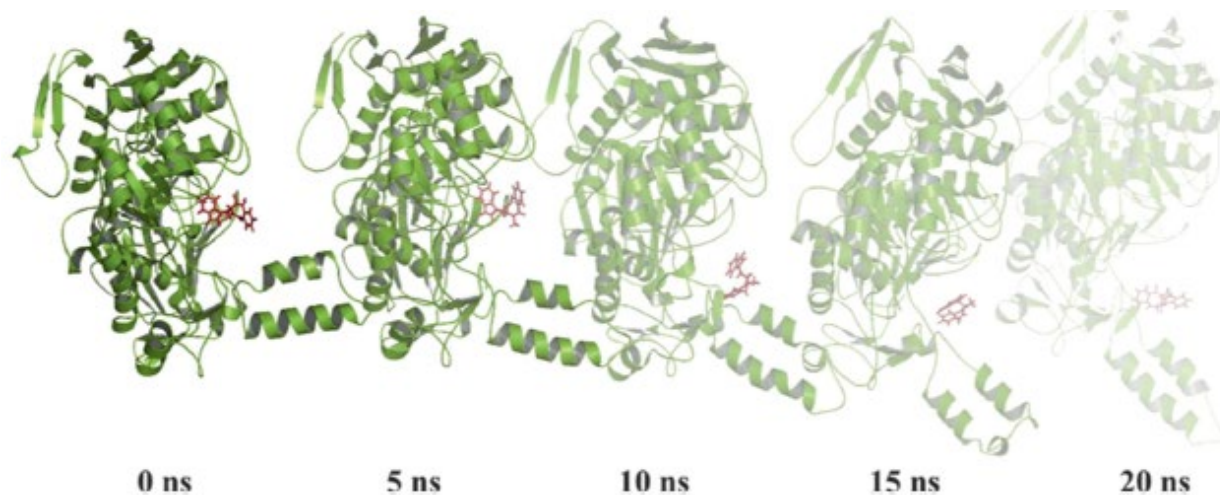

Figure 5. Graphic representation of the MD simulation for the α-glucosidase-4 complex

Materials and methods

General experimental procedures

IR spectra were recorded using a Perkin-Elmer 400 FT-IR or Perkin-Elmer 599B spectrophotometer. NMR spectra, including bidimensional, were recorded in CD$_3$OD or DMSO-d_6 solution on a Bruker Avance III HD (Billerica, MA, USA) or a Varian VNRMS (Palo Alto, CA, USA) spectrometer at 700 MHz (^{1}H) and 175 MHz (^{13}C), using TMS as an internal standard. High-resolution mass spectra, HRMS (DART-TOF+), were acquired with a JEOL AccuTOF JMS-T100LC (Peabody, MA, USA) spectrometer. Optical rotations were obtained with a Perkin-Elmer 241 polarimeter. Preparative HPLC was carried out with a Waters instrument (Milford, MA, USA) equipped with a 2535 pump and a 2998 photodiode array detector, using a Gemini 5u C18 110Å (21.2 × 250 mm) or a Kinetex 5 μm C18 100Å (21.2 × 250 mm) column, and different gradient systems of MeCN and 0.1% aqueous formic acid, at a flow rate of 21.24 ml/min. Control of equipment, data acquisition and processing, and management of chromatographic information were performed using the Empower 3 software.

Column chromatography (CC) was carried out on Sephadex LH-20 (GE Healthcare, Little Chalfont, Buckinghamshire, UK). Flash chromatography was done with a Teledyne CombiFlash Rf+Lumen (Thousand Oaks, CA, USA) chromatograph equipped with a photodiode array detector and an evaporative light-scattering detector, using a RediSep Rf high performance GOLD silica gel column and eluting with a gradient of hexane, chloroform and methanol. Thin-layer chromatographic (TLC) analyses were performed on silica gel 60 F254 plates (Merck, Kenilworth, NJ, USA), and visualized using a $Ce_2(SO_4)_3$ (10%) solution in H_2SO_4.

Fungal material

Malbranchea flavorosea was purchased from the American Type and Culture Collection (ATCC No. 34529). The lyophilized material was resuspended in 5 ml of sterile water and left overnight. Petri dishes containing potato-dextrose agar (Difco PDA, BD, Loveton Circle, Sparks, Maryland, USA) were inoculated using 200 µl of the previous suspension. Stock cultures of the fungus were stored in PDA and monthly subcultured for preservation.

Fermentation, extraction, and isolation

Seed cultures of the fungus were prepared using potato-dextrose broth (Difco PDB) media and incubation at room temperature for 15 days at 200 rpm. Next, M. flavorosea was grown on Erlenmeyer flasks containing 85 g of rice and 200 ml of water (5 × 500 ml). After 30 days of fungal growth, the culture media was exhaustively extracted with 8:2 CH_2Cl_2-MeOH (4 × 500 ml), and the resulting extract was evaporated in vacuo to yield 21.7 g of a brown oily residue. The total extract was suspended in 150 ml of a mixture of MeCN-MeOH (1:1) and partitioned with n-hexane (8 × 150 ml). The combined MeCN-MeOH fractions were dried under vacuum, and the resulting residue (5.9 g) was dissolved in MeOH and subjected to flash chromatography using a gradient of n-hexane-$CHCl_3$ (100:0→0:100, 10 min) and $CHCl_3$-MeOH (100:0, 7.5 min; 100:0→98:2, 7.5 min; 98:2→95:5, 7.5 min; 95:5→90:10, 12.5 min; 90:10→80:20, 20.0 min; 80:20→0:100, 25.0 min). This separation yielded 10 primary fractions (F_A–F_J).

Fraction F_F (540 mg), eluted with $CHCl_3$-MeOH (90:10), was subjected to flash chromatography using a gradient of $CHCl_3$-EtOAc (100:0→0:100, 7.0 min; 0:100, 9.0 min) and EtOAc-MeOH (100:0→99:1, 4.0 min; 99:1→97:3, 5.0 min; 97:3→94:6, 4.0 min; 94:6→90:10, 4.0 min; 90:10 →86:14, 5.0 min; 86:14→80:20, 4.0 min; 80:20→0:100, 3.0 min; 0:100, 15 min;). This separation yielded 7 tertiary fractions (F_{F1}–F_{F7}). Fraction F_{F3} was analyzed by CC eluting with $CHCl_3$-MeOH (3:7) in four fractions (F_{F3a}–F_{F3d}). Fraction F_{F3c} (76 mg) was subjected to preparative RP-HPLC using a gradient of MeCN-0.1% aqueous formic acid (10:90 for 5 min, then 10:90 to 15:85 in 15 min) to yield 5 (8 mg, t_R 10.10 min). Fraction F_{F5} (87 mg) was subjected to preparative RP-HPLC using a gradient of MeCN-0.1% aqueous formic acid (20:80 to 100:0 in 20 min) to yield 2 (1 mg, t_R 8.56 min), 4 (3 mg, t_R 10.53 min), 6 (5 mg, tR 6.16 min) and 7 (1 mg, t_R 5.46 min). Fraction F_G (160 mg), eluted with $CHCl_3$-MeOH (85:15), was subjected to preparative RP-HPLC using a gradient of MeCN-0.1% aqueous formic acid (10:90 to 100:0 in 25 min) to yield 3 (4 mg, t_R 10.11 min). In fractions F_C, F_D, F_E, F_H, and F_I, the previously isolated compounds from this fungus, 8-chloro xylarinol A, xylarinol B, clavatol, flavoroseoside, and massarigenins B and C were chromatographically detected.

Flavoroseoside B (2): colorless glassy solid; $[\alpha]_D^{20}$ + 164.5° (c 0.1, MeOH); UV (λ_{max}) 200.6, 261.8, 312.9 nm; IR (ν_{max}) 3363, 1664, 1614, 1241 cm^{-1}; ^{1}HNMR (700 MHz) and ^{13}C NMR (175 MHz) spectroscopic data in CD$_3$OD, see Table 1; HRMS m/z 361.0684 [M+H]$^+$ (calculated for C$_{15}$H$_{18}$O$_8$Cl 361.0690).

4-Hydroxy-2-O-α-ribofuranosyl-5-methylacetophenone (3): brown oil, $[\alpha]_D^{20}$ + 75.3° (c 0.1, MeOH); UV (λ_{max}) 194.5, 222.4, 326.0 nm; IR (ν_{max}) 3407, 1633, 1264, 1043 cm^{-1}; ^{1}H NMR (700MHz) and ^{13}C NMR (175 MHz) spectroscopic data in CD$_3$OD, see Table 2; HRMS m/z 299.11305 [M+ H]$^+$ (calculated for C$_{14}$H$_{19}$O$_7$ 299.1131).

(S)-3,4-Dihydro-3-(1H-indol-3-ylmethyl)-4-methyl-1H-1,4-benzodiazepine-2,5-dione (4): white amorphous solid, $[\alpha]_D^{20}$ − 57.7° (c 0.1, MeOH); UV (λ_{max}) 214.5, 281.9 nm; IR (ν_{max}) 3229, 1683, 1619, 739 cm^{-1}; ^{1}H NMR (700 MHz) and ^{13}C NMR (175MHz) spectroscopic data in CD$_3$OD, see Table 3; ^{1}H NMR (700 MHz) spectroscopic data in DMSO-d6, see Supplementary Information (Figure S17); HRMS m/z 320.1398 [M + H]$^+$ (calculated for C$_{19}$H$_{18}$O$_2$N$_3$ 320.1399).

Rosigenin (5): colorless glassy solid; ^{1}H NMR (700 MHz, CD$_3$OD) δ 6.88 (1 H, dd, J = 2.5, 10.2 Hz, H-7), 6.01 (1 H, dd, J = 2.9, 10.2 Hz, H-8), 4.82 (1 H, quin, J = 6.5 Hz, H-3), 4.68 (1 H, d, J = 6.5 Hz, H-4), 4.44 (1 H, s, H-10), 3.21 (1 H, m, H-6), 1.36 (3 H, d, J = 6.7 Hz, H-11), 1.28 (3 H, d, J = 7.2 Hz, H-12); ^{13}C NMR (175MHz, CD$_3$OD) δ 199.1 (C-9), 178.4 (C-1), 154.1 (C-7), 125.4 (C-8), 81.8 (C-3), 76.9 (C-10), 75.6 (C-4), 61.9 (C-5), 34.9 (C-6), 18.8 (C-12), 14.6 (C-11).

Massarilactone B (6): white amorphous solid; ^{1}H NMR (700 MHz, CD$_3$OD) δ 5.88 (1 H, qdd, J = 0.8, 6.4, 12.8 Hz, H-12), 5.76 (1 H, m, J = 1.2, 8.4, 16.4 Hz, H-11), 4.92 (1 H, qd, J = 1.3, 6.8 Hz, H-3), 4.82 (1 H, dd, J = 4.0, 8.2 Hz, H-6), 4.25 (1 H, dd, J = 1.4, 3.7 Hz, H-8), 3.77 (1 H, dd, J = 3.7, 4.1 Hz, H-7), 1.71 (3 H, dd, J = 0.9, 6.4 Hz, H-13), 1.41 (3 H, d, J = 6.8 Hz, H-10). ^{13}C NMR (175MHz, CD$_3$OD) δ 179.3 (C-4), 174.1 (C-1), 133.1 (C-12), 126.7 (C-11), 100.8 (C-9), 86.3 (C-6), 75.5 (C-3), 72.6 (C-7), 64.1 (C-8), 17.9 (C-13), 17.8 (C-10).

Riboxylarinol B (7): colorless glassy solid; ^{1}H NMR (700 MHz, CD$_3$OD) δ 7.11 (1 H, t, J = 7.7 Hz, H-5), 6.74 (1 H, d, J = 7.4 Hz, H-6), 6.67 (1 H, d, J = 7.9 Hz, H-4), 5.38 (1 H, m, H-1′), 5.09 (1 H, dd, J = 2.6, 11.9 Hz, H-6′a), 4.98 (1 H, dd, J = 5.8, 11.9 Hz, H-6′b), 3.72 (1 H, m, H-4′), 3.66 (1 H, m, H-3′), 2.09 (1 H, ddd, J = 3.6, 4.8, 14.3 Hz, H-2′a), 1.79 (1 H, dt, J = 8.3, 14.3 Hz, H-2′b), 1.20 (3 H, d, J = 6.4 Hz, H-5′); ^{13}C NMR (175 MHz, CD$_3$OD) δ 152.8 (C-3), 145.2 (C-1), 130.4 (C-5), 125.8 (C-2), 114.8 (C-6), 113.2 (C-4), 84.3 (C-1′), 74.8 (C-4′), 71.5 (C-3′), 71.4 (C-6′), 40.1 (C-2′), 18.5 (C-5′).

3,4-Dihydro-3-(1H-indol-3-ylmethyl)-1-methyl-1H-1,4-benzodiazepine-2,5-dione (9): white solid, mp. 217–219 °C; $[\alpha]_D^{20}$ − 89.9° (c 0.1, MeOH); UV (λ_{max}) 214.5, 281.9 nm; IR (ν_{max}) 3340, 1650, 1463, 741 cm^{-1}; ^{1}H NMR (700 MHz) and ^{13}C NMR (175MHz) spectroscopic data in CD3OD, see Table 3; HRMS m/z 320.1399 [M + H]$^+$ (calculated for C$_{19}$H$_{18}$O$_2$N$_3$ 320.1399).

Synthesis of compound 9

A mixture of N-methylisatoic anhydride (555 mg), D-tryptophan (575 mg), triethylamine (500 μl) and H_2O (8 ml) was stirred at room temperature for 5 h; then the volatile material was removed in vacuo. To the resulting residue, glacial acetic acid (12 ml) was added, the solution was then refluxed for 8 h. The reaction mixture was concentrated in vacuo and partitioned with EtOAc and H_2O. The organic layer was washed with a solution of $NaHCO_3$, followed by H_2O (10 ml × 2) and then dried over anhydrous Na_2SO_4. Finally, the solvent was removed in vacuo to yield 450 mg of crude 9. The crude was recrystallized from MeOH (30 ml) to yield 360 mg of compound 9.

Enzymatic assay

Two types of enzymes were used in the enzymatic assay, α-glucosidase from R. obeum (α-Ro) and α-glucosidase from S. cerevisiae (α-GHY). For α-Ro assay, compounds 2–6, 9 and acarbose (positive control) were dissolved phosphate buffer solution (PBS, 25 mM, pH 7). For α-GHY assay, compounds 4, 9 and acarbose were dissolved in MeOH or phosphate buffer solution (PBS, 100 mM, pH 7). Aliquots of 0-20 μl of testing materials (triplicated) were incubated for 10 min with enzyme solution (5 μl of 5.2 mg/ml α-Ro enzyme in PBS or 20 μl of 1 U/ml α-GHY enzyme in PBS). After incubation, 10 μl of p-nitrophenyl-α-D-glucopyranoside (20mM for α-Ro and 5 mM for α-GHY) were added and further incubated for 20 min for α-GHY or 3 h for α-Ro at 37 °C, and the absorbance measured at 415 nm. The inhibitory activity was determined as a percentage compared to the blank according to the following equation:

$$\%R.\,obeum\;\alpha-\text{glucosidase} = \left(1 - \frac{A_{415b}}{A_{415c}}\right) \times 100\%$$

where % R. obeum α-glucosidase is the percentage of inhibition, A_{415c} is the corrected absorbance of the samples under testing ($A_{415\;end} - A_{415\;initial}$), and A_{415b} is the absorbance of the blank ($A_{415\;end\;blank} - A_{415\;initial\;blank}$). All assays were performed by triplicated. The IC_{50} was calculated by regression analysis, using the following equation:

$$\%\text{Inhibition} = \frac{A_{100}}{1 + \left(\frac{1}{IC_{50}}\right)^{s}}$$

where A_{100} is the maximum inhibition, I is the inhibitor concentration, IC_{50} is the concentration required to inhibit activity of the enzyme by $50\% \pm SD$, and s is the cooperative degree.

Docking protocol

Docking was done using the Protein Data Bank X-ray structure of α-glucosidase from R. obeum (3PHA.pdb); the structures of 1–9 were constructed using HyperChem 8 software (Hypercube Inc., Gainesville, FL) and later minimized using Gaussian 09, revision A.02 (Gaussian Inc., Wallingford, CT) at DFT B3LYP/3-21G level of theory. AutoDockTools 1.5.4 (http://mgltools.scripps.edu/) was used to prepare the pdb files of α-glucosidase and the compounds. All hydrogen atoms and the Kollman united-atom partial charges were added to the protein structures, while Gasteiger-Marsili charges and rotatable groups were automatically assigned to the structures of the ligands. Blind docking was carried out with AutoDock 4.2 (http://autodock.scripps.edu/) [25, 26] using the default parameters for the Lamarkian genetic algorithm. Electrostatic grid maps were generated for each atom type using the auxiliary program AutoGrid 4 that is part of AutoDock 4.2. The initial grid box size was 60 Å × 60 Å × 60 Å in the

x, y, and z dimensions. Afterwards, a refined docking analysis was performed with a smaller grid box of 30 Å × 30 Å × 30 Å, centered at the previously identified ligand's-binding site. Docking was evaluated with AutoDockTools 1.5.4 using cluster analysis, and the PyMOL software (Schrödinger, Cambridge, MA) [27].

Molecular dynamics simulation

The complexes resulting from the docking study were processed with antechamber toolkit to generate suitable topologies for the LEaP module from AMBER 14 [28, 29]. Each structure and complex were subjected to the following protocol: hydrogens and other missing atoms were added using the LEaP module with the parm99 parameter set, Na+ counter ions were added to neutralize the system; the structures were then solvated in an octahedral box of explicit TIP3P model water molecules localizing the box limits at 12 Å from the protein surface. The total number of atoms in the simulated system was ~70,000, including solvent molecules. MD simulations were performed at 1 atm and 298 K, during 20 ns. They were maintained with the Berendsen barostat and thermostat, using periodic boundary conditions and particle mesh Ewald sums (grid spacing of 1 Å) for treating long-range electrostatic interactions with a 10 Å cutoff for computing direct interactions. The SHAKE algorithm was used to satisfy bond constraints, allowing to use a 2 fs time step for the integration of Newton's equations as recommended in the AMBER package [28, 30]. Amber ff99SB and gaff force field [28, 31] parameters were used for all amino acid and organic molecules, respectively. The protocol consisted in performing an optimization of the initial structure, followed by a 50 ps heating step at 310 K, 50 ps for equilibration at constant volume and 500 ps for equilibration at constant pressure. Three independent 20 ns MD simulations were performed. Frames were saved at 100 ps intervals for subsequent analysis. The analyses were conducted with cpptraj [32] on the trajectory time intervals where the convergence criteria were met. We monitored the total energy of the system (including solvation) during the simulations and the pairwise mass-weighted RMSD on the alpha carbons backbone; C and N atoms were used as a metric. Binding free energies calculated by molecular mechanics/Poisson–Boltzmann surface area (MM/PBSA) [33, 34].

Conflict of interest. The authors declare that they have no conflict of interest.

References

1. International Diabetes Federation. IDF Diabetes Atlas, 8th edn. Brussels, Belgium:International Diabetes Federation, 2017.

2. Ghani U. Re-exploring promising α-glucosidase inhibitors for potential development into oral anti-diabetic drugs: Finding needle in the haystack. Eur J Med Chem. 2015;103:133–62.

3. Mata R, Figueroa M, Rivero-Cruz I, Macías-Ruvalcaba ML. Insights in fungal bioprospecting in Mexico. Planta Med. 2018;84:594–605. https://doi.org/10.1055/s-0044-101551

4. Mata R, Cristians S, Escandón-Rivera S, Juárez-Reyes K, Rivero-Cruz I. Mexican antidiabetic herbs: valuable sources of inhibitors of α-glucosidases. J Nat Prod. 2013;76:468–83.

5. Verástegui-Omaña B, et al. α-Glucosidase inhibitors from Malbranchea flavorosea. J Nat Prod. 2017;80:190–5.

6. Sigler L, Carmichael JW. Taxonomy of Malbranchea and some other hyphomycetes with artroconidia. Mycotaxon . 1976;4:349–488.

7. Wijayawardene NN, et al. Notes for genera: Ascomycota. Fungal Divers. 2017;86:1–594.

8. Currah RS. Taxonomy of the Onygenales: Arthrodermataceae, Gymnoascaceae, Myxotrichaceae and Onygenaceae. Mycotaxon. 1985;24:1–216.

9. Sarrocco S, et al. A polyphasic contribution to the knowledge of Auxarthron (Onygenaceae). Mycol Prog. 2015;14:112.

10. Schoch CL, et al. Nuclear ribosomal internal transcribed spacer (ITS) region as a universal DNA barcode marker for Fungi. Proc Natl Acad Sci USA. 2012;109:6241–6.

11. Raja HA, Miller AN, Pearce CJ, Oberlies NH. Fungal identification using molecular tools: a primer for the natural products research community. J Nat Prod. 2017;80:756–70.

12. Hambleton S, Egger KN, Currah RS. The genus Oidiodendron: species delimitation and phylogenetic relationships based on nuclear ribosomal DNA analysis. Mycologia. 1998;90:854–68.

13. Min YJ, et al. Diversity and saline resistance of endophytic fungi associated with Pinus thunbergii in coastal shelterbelts of Korea. J Microbiol Biotechnol. 2014;24:324–33.

14. Bonito G, et al. Isolating a functionally relevant guild of fungi from the root microbiome of Populus. Fungal Ecol. 2016;22: 35–42.

15. Cannon PF, Kirk PM. Fungal families of the world. United Kingdom: Centre for Agricultural Bioscience International; 2007.

16. Okada K, et al. Ubiquinone system, GC contents and cellular fatty acid composition of species of the form-genus Malbranchea and Coccidioides immitis for chemotaxonomic study. Mycoscience . 1995;36:385–9.

17. Albinati A, Bruckner S, Camarda L, Nasini G. Rosigenin, an unusual metabolite from Mycosphaerella rosigena. Tetrahedron. 1980;36:117–21.

18. Oh H, Swenson DC, Gloer JB, Shearer CA. Massarilactones A and B: novel secondary metabolites from the freshwater aquatic fungus Massarina tunicata. Tetrahedron Lett. 2001;42:975–7.

19. Mullapudi V, Ramana CV. The total synthesis and structural assignment of hexaketide xylarinol B and its C1'-epimer. Asian J Org Chem. 2016;5:417–22.

20. Pan C, et al. New compounds from a hydrothermal vent crab-associated fungus Aspergillus versicolor XZ-4. Org Biomol Chem. 2017;15:1155–63.

21. Kusano M, et al. Nematicidal alkaloids and related compounds produced by the fungus Penicillium cf. simplicissimum. Biosci Biotechnol Biochem. 2000;64:2559–68.

22. Flores-Bocanegra L, González-Andrade M, Bye R, Linares E, Mata R. α-Glucosidase inhibitors from Salvia circinata. J Nat Prod. 2017;80:1584–93.

23. Shan WG, et al. α-Glucosidase inhibitors from the fungus Aspergillus terreus 3.05358. Chem Biodivers. 2015;12:1718–24.

24. Del Valle P, Martínez AL, Figueroa M, Raja HA, Mata R. Alkaloids from the fungus Penicillium spathulatum as α-glucosidase inhibitors. Planta Med. 2016;82:1286–94.

25. Morris GM, et al. Automated docking using a Lamarckian genetic algorithm and an empirical binding free energy function. J Comput Chem. 1998;19:1639–62.

26. Huey R, Morris GM, Olson AJ, Goodsell DS. A semiempirical free energy force field with charge-based desolvation. J Comput Chem. 2007;28:1145–52.

27. The PyMOL Molecular Graphics System, Version 2.0 Schrödinger, LLC. https://pymol.org/

28. Case DA, et al. AMBER 12. San Francisco: University of California; 2012.

29. Case DA, et al. The Amber biomolecular simulation programs. J Comput Chem. 2005;26:1668–88.

30. Walker RC, Crowley MF, Case DA. The implementation of a fast and accurate QM/MM potential method in Amber. J Comput Chem. 2008;29:1019–31.

31. Lindorff-Larsen K, et al. Improved side-chain torsion potentials for the Amber ff99SB protein force field. Proteins. 2010;78:1950–8.

32. Roe DR, Cheatham TE. PTRAJ and CPPTRAJ: software for processing and analysis of molecular dynamics trajectory data. J Chem Theory Comput. 2013;9:3084–95.

33. Treesuwan W, Hannongbua S. Bridge water mediates nevirapine binding to wild type and Y181C HIV-1 reverse transcriptase--evidence from molecular dynamics simulations and MM-PBSA calculations. J Mol Graph Model. 2009;27:921–9.

34. Zhou Z, Madura JD. Relative free energy of binding and binding mode calculations of HIV-1 RT inhibitors based on dock-MMPB/GS. Proteins. 2004;57:493–503.